# Mapping Polysulfides in Sodium-Sulfur Batteries

*Esther Lilian Gray*[1], *Jung-In Lee*[1], *Zhuangnan Li*[1], *James Moloney*[1], *Ziwei Jeffrey Yang*[1], *Manish Chhowalla*[1*]

[1]Department of Materials Science and Metallurgy, University of Cambridge, Cambridge, CB30FS, UK

*Corresponding author.

Email: mc209@cam.ac.uk (Manish Chhowalla)

**Abstract**

Sodium-sulfur (Na-S) batteries provide lithium-free alternatives to lithium-sulfur (Li-S) batteries. Na-S chemistry has been less studied. Thus, the types of polysulfides (PS) and their evolution during charge-discharge of Na-S batteries are not as well understood as in the Li-S system. We therefore study the formation of different PS in tetraethylene glycol dimethyl ether (TEGDME)-based electrolyte during battery operation using *in-situ* Raman and *ex-situ* ultraviolet-visible (UV-Vis) spectroscopies. We start by making reference solutions with different ratios of $Na_2S$ to sulfur, ranging from pure $Na_2S$ to $Na_2S$:7S, with sulfur ratio increasing by one integer per solution. We then correlate the UV-Vis and Raman peaks to PS species. Our galvanostatic charge-discharge (GCD) and cyclic voltammetry (CV) measurements show a total of ten features. Using *ex-situ* UV-Vis on aliquots and *in-situ* Raman spectra from PS solutions at GCD voltage plateaus, we map out sodium polysulfide (NaPS) species at key stages of the charge-discharge cycle. We identify $Na_2S_8$, $Na_2S_4$, $Na_2S_2$ as intermediates and $Na_2S$ as the final product. We find that the intermediate $Na_2S_6$ forms from disproportionation of $Na_2S_8$ and $Na_2S_4$. We also observe that intermediate polysulfides can also dissociate into $S_3^{\bullet-}$ radical species which contributes to loss of active material. Our results provide detailed insights into Na-S chemistry that will be helpful for the development of high performance and stable batteries.

**Keywords:** sodium-sulfur batteries, sodium polysulfides, tetraethylene glycol dimethyl ether, *in-situ* Raman spectroscopy, *ex-situ* UV-vis spectroscopy, $S_3^{\bullet-}$ radical species.

Lithium-ion (Li-ion) batteries are currently low in energy density and contain critical metals.[1] The use of sulfur as a cathode and lithium metal as an anode offers the possibility of achieving high energy density without the need for critical materials in applications requiring high energy density batteries.[2] Sodium-sulfur (Na-S) batteries are interesting for the same reason as Na ion batteries – they offer an alternative to lithium-based batteries, which may have cost advantages in some applications such as large-scale grid energy storage.[3]

However, Na-S batteries face several challenges that are similar to Lithium-sulfur (Li-S) batteries. These include polysulfide (PS) shuttling, cyclability, dendrite growth, and volume expansion of sodium. New separator designs,[4-6] electrolytes,[7-11] and cathodes[12-14] or catholytes[15] have been reported to address some of these challenges. Studies have also focused on reaction pathways involved in the formation and decomposition of sodium polysulfides (NaPS) during cycling.[11, 16] Most studies use ether-based electrolytes and *ex-situ* characterization techniques.[8, 17, 18] *In-situ* analysis has been done for Na-S batteries with carbonate electrolytes or catholytes.[7, 15, 19, 20] In particular, Xu et al. used *in-situ* Raman to monitor the formation of $Na_2S_x$ from 2.70 V to 1.20 V discharge voltage.[7] However, further insights into voltages at which various polysulfides form and reduce during cycling could be useful for optimizing the performance of Na-S batteries through improved electrode or electrolyte design.

Understanding PS reactions may identify critical rate-determining steps and capacity loss mechanisms during cycling. During discharge, elemental sulfur is converted into successively smaller liquid phase NaPS ($Na_2S_n$, $4 \leq n \leq 8$) and then finally to solid $Na_2S_2$ and $Na_2S$.[21] However, the slow formation kinetics of solid sodium sulfides restrict discharge efficiency and lead to irreversible capacity loss during cycling.[21] The commonly observed discharge capacity of Na-S batteries (1050 mA h $g^{-1}$) falls between theoretical capacities of forming $Na_2S_2$ and $Na_2S$ [21] as the final product. However, it is not clear what the final discharge products are in

experimental cells.[21] Some reports suggest a mixture of $Na_2S_2$ and $Na_2S$ or $Na_2S_3$ and $Na_2S_2$.[8, 21, 22] Previous Na-S studies using a tetraethylene glycol dimethyl ether (TEGDME) electrolyte[8, 15, 17, 18, 20, 23] have reported $S_6^{2-} \leftrightarrow 2S_3^{\bullet-}$ contributes significantly to the loss in active material.

Here, we investigate Na-S batteries with metallic $MoS_2$ nanosheet electrodes as a sulfur host, 1 M Sodium trifluoromethanesulfonate ($NaCF_3SO_3$) in TEGDME as the electrolyte, and sodium metal as the anode. The aim is to study PS products using *ex-situ* UV-Vis spectroscopy and *in-situ* Raman spectroscopy. Using these methods, we identify $Na_2S_8$, $Na_2S_4$, $Na_2S_2$ as intermediates and $Na_2S$ as the final product. Our results also suggest that the intermediate $Na_2S_6$ does not form directly from the reduction of sulfur but from disproportionation of $Na_2S_8$ and $Na_2S_4$. Dissociation of $Na_2S_6$ or the disproportionation of $Na_2S_4$ leads to the formation of $S_3^{\bullet-}$ radical species which contributes to loss of active material.

## Results and discussion

### Battery charge/discharge

A Na-S battery was assembled using sulfur dispersed on metallic $MoS_2$ host, sodium anode and 1 M $NaCF_3SO_3$ TEGDME as the electrolyte (see Experimental Methods for preparation of the cathode and Supplementary Information for characterization of material in Figure S1). We have previously reported that the metallic $MoS_2$ is a good host for Li-S batteries.[24] We therefore investigate its suitability as a cathode host for the Na-S battery system. The experimental details for coin cell manufacture are described in the Experimental Methods section. The first galvanic charge-discharge (GCD) cycle voltage profiles are presented in Figure 1a, along with the corresponding cyclic voltammetry (CV) plot in Figure 1b. The capacity of this coin cell was found to be ~ 600 mA h $g^{-1}$ with other cells performing within a standard deviation of ± 150 mA h $g^{-1}$ (Refer to Figure S2a for the GCD of the first cycle across five cells). The typical cycling performance of Na-S batteries with metallic $MoS_2$ cathode hosts is shown in Supplementary Information Figure S2b. The corresponding impedance measurements in Supplementary Information Figure S2c show that the resistance of the cell increases with cycling. Several CV plots showing how the plateaus and peaks change with cycling are provided in Supplementary Information Figures S2d and S2e with differential capacity curves of first cycle in Figure S2f.

Figure 1a shows that during charging, the plateaus occur at 1.85 V, 1.95 V, 2.35 V and 2.60 V, while features occur at 2.30 V, 1.90 V, 1.60 V and lower voltages in the discharge curve. The CV plot replicates these plateaus in the form of oxidation and reduction peaks as shown in Figure 1b. The curves in Figure 1a are similar to previous Na-S battery studies.[8, 15, 17, 18, 23] Typically, ~ 2.30 V and 1.60 V plateaus are attributed to liquid-liquid conversion reaction of $Na_2S_8$ to $Na_2S_4$. Voltages 1.60 V to 1.10 V correspond to liquid-solid conversion reaction of $Na_2S_2$ and $Na_2S$.[11, 25] It has also been noted that the TEGDME solvent encourages the

disproportionation of $S_4^{2-}$ and dissociation of $S_6^{2-}$ to $S_3^{\bullet-}$ radical, which causes loss of active material.[23]

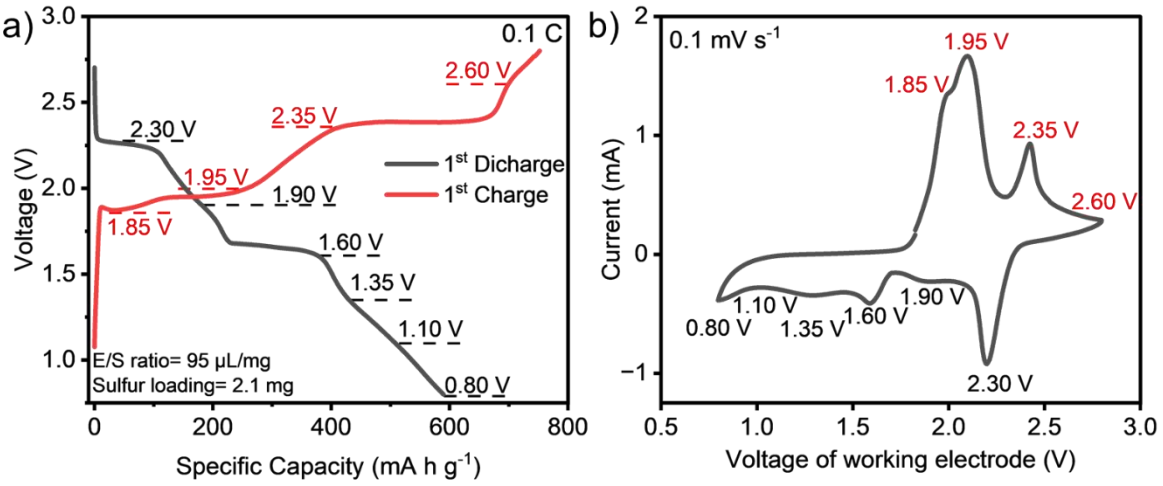


**Figure 1.** a) The galvanic charge-discharge (GCD) of 1st cycle at 0.1 C rate achieving initial capacity of 600 mA h per gram ($g^{-1}$) of sulfur and b) cyclic voltammetry (CV) plot of Na-S battery with metallic phase $MoS_2$ nanosheets as sulfur cathode host and 1.0 M $NaCF_3SO_3$ TEGDME electrolyte. The plateaus in GCD curves correspond to the peaks in the CV curves (red = charge and black = discharge) between a working voltage of 2.6 V to 0.80 V.

**UV-Vis on reference solutions of sodium polysulfides**

For UV-Vis and Raman spectroscopies, 0.2 M solutions of liquid-phase NaPS were prepared in the electrolyte (see Experimental Methods for details). Figure 2a shows photographs of the reference solutions of liquid-phase NaPS with a concentration of 0.2 M $Na_2S_n$ ($n$ ranging from 1 to 8) with different compositions. These solutions serve as references with predetermined ratios between S and $Na_2S$. UV-Vis spectra of these reference solutions are shown in Figure 2b (see Figure S3 and Table S1 for detailed UV-Vis results). These spectra provide an indication of the peaks corresponding to various polysulfides that form during cycling of a battery.

The various peaks observed in UV-Vis spectra (Figure 2b) from the reference liquid-phase PS solutions are labelled in Table 1.[23, 26-33] The spectra show that the concentration of shorter chain polysulfides increases when the sodium-to-sulfur ratio is increased. The results also indicate that different PS species coexist. Thus, the labels refer to the sodium-to-sulfur ratio of the prepared solutions rather than the absolute concentration of PS species.

We observe 3 consistent peaks and 2 distinct regions in the UV-Vis spectra. We label the regions as A and B and the 3 consistent peaks are labelled as $S^{2-}$, $S_8^{2-}$ and $S_7^{2-}$ and $S_3^{\bullet-}$ for clarity. The first peak at around 267 nm corresponds to the $S^{2-}$ PS.[27] $S_8^{2-}$ and $S_7^{2-}$ are characterized by peaks in the range of 285-290 nm.[28] These peaks are the strongest for $Na_2S$:7S and $Na_2S$:6S solutions. The shoulder next to the $S_8$ and $S_7^{2-}$ peak is hypothesized to correspond to $S_8^{2-}$, $S_7^{2-}$, or $S_6^{2-}$ species, as it is consistently observed in all three solutions ($Na_2S$:7S, $Na_2S$:6S, and $Na_2S$:5S). However, further work is necessary to definitively assign this peak. The $S_4^{2-}$ species show absorption at 360 nm (region A) and 450 nm (region B), while $S_6^{2-}$ is identified by peaks at 350 nm (region A) and 460 nm (region B).[27, 29, 34] The 450 nm and 460 nm were observed in $Na_2S$:3S solution. However, only the 460 nm peak was present in $Na_2S$:3S, $Na_2S$:4S, and $Na_2S$:5S solutions. Additionally, $Na_2S$:S and $Na_2S$:2S show a peak at 430 nm which was deduced to be from $S_2^-$ species.[27, 30] Finally, the radical species $S_3^{\bullet-}$ may be attributed to the absorption peak at 620 nm.[23, 26, 27, 29, 31, 33]

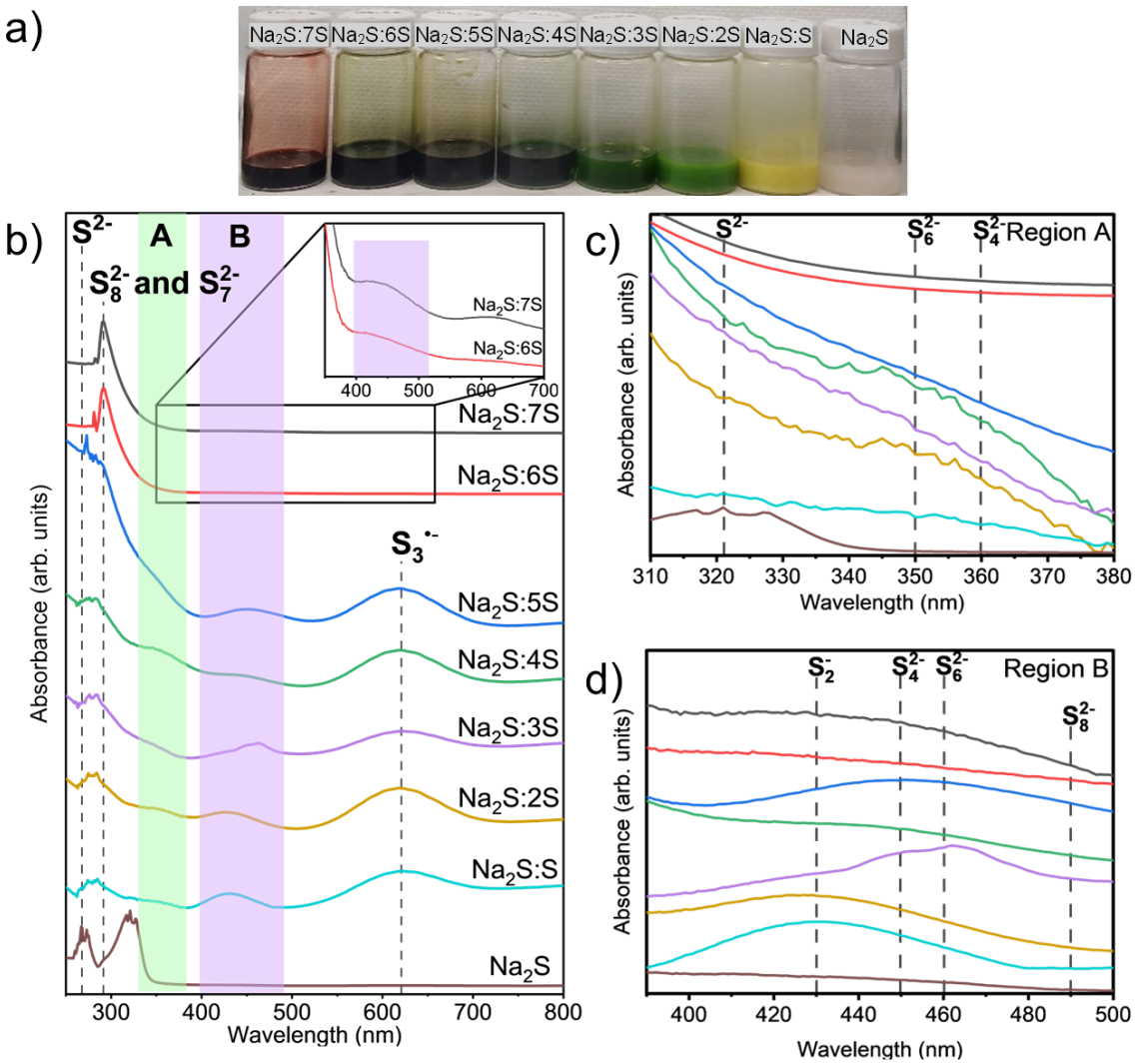


**Figure 2.** a) Photographs of 0.2 M NaPS solutions in 1.0 M $NaCF_3SO_3$ and TEGDME. Solutions are labelled with different molar ratios of sulfur to $Na_2S$. b) UV-Vis spectra of the reference PS solutions in 1.0 M $NaCF_3SO_3$ in TEGDME. Consistent peaks are labelled individually with regions A and B containing multiple peak shifts. c) is zoomed in region A and d) region B, both identifying the individual peaks within the respective regions and the responsible species are summarised in Table 1.

**Table 1.** PS identification from UV-Vis spectra. Three consistent peaks and two distinct regions labelled in Figure 2 were used to identify the PS species.

| Wavelength (nm) | Sample containing peak/ region | Polysulfide Species |
|---|---|---|
| **267** | $Na_2S$ | $S^{2-}$ |
| **285-290** | $Na_2S$:7S | $S_8^{2-}$ and $S_7^{2-}$ |
| | $Na_2S$:6S | |
| | $Na_2S$:5S | |
| | $Na_2S$:4S | |
| | $Na_2S$:3S | |
| | $Na_2S$:2S | |
| | $Na_2S$:S | |
| **Region A** **320-360** | $Na_2S$:5S | $S^{2-}$, $S_4^{2-}$, $S_6^{2-}$ |
| | $Na_2S$:4S | |
| | $Na_2S$:3S | |
| | $Na_2S$:2S | |
| **Region B** **430-460** | $Na_2S$:5S | $S_2^{-}$, $S_4^{2-}$, $S_6^{2-}$, $S_8^{2-}$ |
| | $Na_2S$:4S | |
| | $Na_2S$:3S | |
| | $Na_2S$:2S | |
| | $Na_2S$:S | |
| **620** | $Na_2S$:5S | $S_3^{\bullet-}$ |
| | $Na_2S$:4S | |
| | $Na_2S$:3S | |
| | $Na_2S$:2S | |

**Raman on reference solutions of sodium polysulfides**

Additional identification of NaPS was conducted with Raman spectroscopy. Raman spectra of reference liquid-phase PS solutions are shown in Figure 3. NaPS corresponding to the Raman peaks are summarised in Table 2 (see also Supplementary Information Figure S4). The Raman spectra mostly agree with UV-Vis results and also show that several PS species coexist in the reference solutions. In contrast to UV-Vis, Raman indicated that $Na_2S$ is present in almost all compositions, which can be attributed to undissolved $Na_2S$. Further, the NaPS species are more distinguishable with Raman spectroscopy.

Specific peaks observed in Raman and shown in Figure 3a are attributed to different NaPS species. The $S^{2-}$ species (▽) exhibit distinct peaks at 119 $cm^{-1}$ and 255 $cm^{-1}$.[35-37] The peak at 192 $cm^{-1}$ is attributed to the $S_2^{2-}$ species (▲).[38] The $S_3^{2-}$ species (□) peaks are observed at 132 $cm^{-1}$, 208 $cm^{-1}$, and 450 $cm^{-1}$.[39-42] The $S_4^{2-}$ species (●) have characteristic peaks at 390 $cm^{-1}$ and 518 $cm^{-1}$.[37, 39, 43, 44] Additionally, the $S_6^{2-}$ species (○) are identified by peaks at 386 $cm^{-1}$ and 440 $cm^{-1}$,[40, 41, 45] while the $S_8^{2-}$ species (★) show peaks at 380 $cm^{-1}$ and 436 $cm^{-1}$.[41-43] The radical species $S_3^{\bullet-}$ (☆) can be recognized by the symmetric stretching mode at 534 $cm^{-1}$.[37, 41, 43, 44, 46-49] Thus, the Raman peaks provide insight into various NaPS species present in different states (see Supplementary Information Table S2).

Additional observations of the $S_3^{\bullet-}$ radical signal intensity were made across different NaPS solutions. The radical signal is most prominent in $Na_2S$:6S, $Na_2S$:5S, and $Na_2S$:4S, which can be attributed to its formation via the disproportionation of $Na_2S_4$ or the dissociation of $Na_2S_6$.[40, 50, 51] These processes are dictated by the $Na_2S$:nS ratio, governed by thermodynamic equilibrium and stoichiometric constraints, ultimately influencing the predominant polysulfide species in solution.[40, 50, 51]

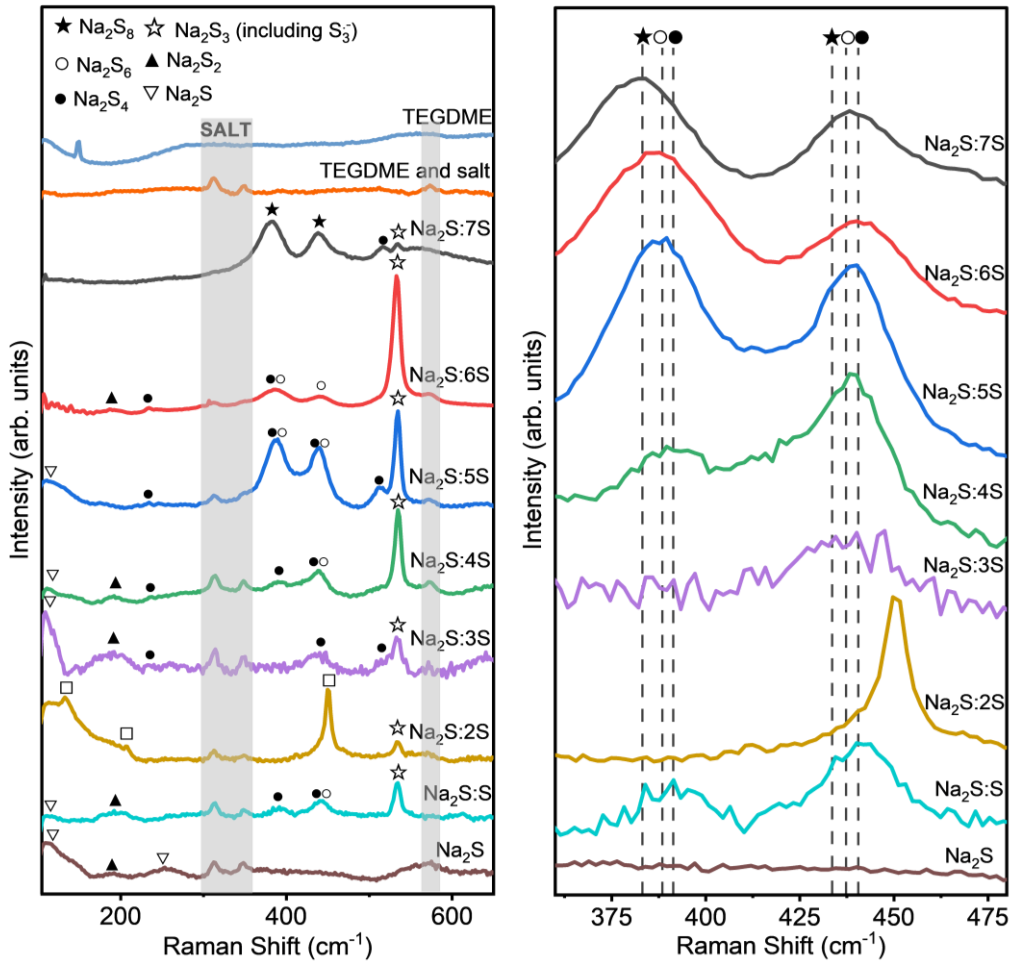


**Figure 3.** a) Raman spectra of PS solutions used as references in 1.0 M $NaCF_3SO_3$ and TEGDME with labels identifying each peak with a PS. Vertical shaded regions identify salt and TEGDME peaks. b) The zoomed in region between 350 to 480 $cm^{-1}$, shows peaks around 380 $cm^{-1}$, 386 $cm^{-1}$ and 390 $cm^{-1}$ corresponding to $S_8^{2-}$ and $S_7^{2-}$, $S_6^{2-}$, and $S_4^{2-}$ respectively. Peaks at 436 $cm^{-1}$, 440 $cm^{-1}$ and 442 $cm^{-1}$ also correspond to these species, with shifts in peak positions reflecting changes in concentration as indicated by the vertical dashed lines and associated symbols. Figure b also shows that the relative intensity ratios of the two peaks also change with concentration.

**Table 2.** Wavenumbers of Raman peaks associated with different PSs in solution (different symbols correspond to those in Figure 3).

| Polysulfide (symbol) | Wavenumber(s) ($cm^{-1}$) |
|---|---|
| $S^{2-}$ (▽) | 119, 255 |
| $S_2^{2-}$ (▲) | 192 |
| $S_3^{2-}$ (□) | 132, 207, 450 |
| $S_4^{2-}$ (●) | 234, 390, 442, 518 |
| $S_6^{2-}$ (○) | 386, 440 |
| $S_8^{2-}$ and $S_7^{2-}$ (★) | 380, 436 |
| $S_3^{\bullet-}$ (Symmetric stretching mode) (☆) | 534 |

***Ex-situ* UV- vis spectroscopy of solutions at different voltage plateaus**

To understand the evolution of NaPS during battery operation, a Na-S cell was cycled under galvanostatic conditions (0.1 C rate), beginning with a discharge step (see set up in Supplementary Information Figure S5). The discharge process was paused at the voltage plateaus indicated in Figure 1a to obtain aliquots of the electrolyte for UV-Vis measurements. The UV-Vis spectra from the first discharge are shown in Figure 4a. The results were interpreted based on the assigned peaks from reference solutions. The results of the first discharge cycle (Figure 4a) show two peaks at 2.30 V between 285-290 nm, which are attributed to the $S_8^{2-}$ and $S_7^{2-}$ species. This suggests that between 2.60 to 2.30 V, the conversion of $S_8$ to $Na_2S_8$ /N $a_2S_7$ occurs. Additionally, a peak at 310 nm (labelled "*x*") is present, indicating the presence of cyclic $S_8$, similar to what has been reported by Han et al.[27] at 2.30 V. At 1.90 V, a broad peak centered at 360 nm emerges, indicating the formation of $S_4^{2-}$ species. This peak becomes asymmetrical and sloped from 1.55 V onwards, continuing to increase as the

battery discharges further. The results suggest the formation of $S_6^{2-}$ species, while $S_4^{2-}$ remains, as indicated by an incline at 450 nm and the persistent 360 nm peak. This suggests that both $S_6^{2-}$ and $S_4^{2-}$ species are increasing in concentration within the electrolyte. It is inferred that the PS $S_6^{2-}$ dissipates in the electrolyte and it may contribute to battery capacity fading. At 1.55 V, along with the formation of $S_6^{2-}$ species, aliquots begin to show a peak at 620 nm, indicating the presence of the $S_3^{\bullet-}$ radical. From the simultaneous appearance of $S_6^{2-}$ and the $S_3^{\bullet-}$ radical, it is inferred that the $S_3^{\bullet-}$ radical is formed either from the dissociation of $Na_2S_6$ or the disproportionation of $Na_2S_4$.[8, 15, 17, 18, 20, 23] There is an observed change in the broadness of the peak at ~350–360 nm from 1.35 V to 1.10 V and 0.80 V. At 1.35 V, the peak is asymmetric, suggesting an equilibrium between $Na_2S_6$ and $Na_2S_4$. By 1.10 V, the peak becomes more symmetric, indicating a dominance of $Na_2S_4$. This could potentially result from $Na_2S_6$ dissociating into $Na_2S_3$ at lower potentials. Finally, a peak at 267 nm, attributed to $Na_2S$, becomes evident at 1.10 V.

We also performed the same analysis during the 1st charge cycle (Supplementary Information Figure S6a). We found that the peak associated with $S_3^{\bullet-}$ radical increases, while the peaks at 267 nm and 350 nm are observed throughout. This suggests that $S_6^{2-}$, $S_3^{\bullet-}$ radical and $Na_2S$ polysulfides in the electrolyte are present throughout. However, it should be noted that UV-Vis from not all aliquots was measurable because the PS conversion reaction is concentrated at the surface of the electrode and the aliquots were taken from bulk electrolyte solutions. Consequently, it was not possible to differentiate minor changes in concentration of each reaction in the small volume aliquots compared to measurements on bulk solutions.

We also measured the NaPS concentrations after 6th discharge and charge cycles (Figure 4b and Supplementary Information Figure S6b, respectively) to observe any changes in the concentration of $Na_2S_6$, the $S_3^{\bullet-}$radical, and $Na_2S$ species. In the 6th discharge data, an

additional peak at 325 nm (labelled "*y*") appears at 1.90 V but disappears at lower voltages. This peak has been assigned to the $S_3^{2-}$ species based on Ref [27], and it also appears in the 6$^{th}$ charge data at 1.78 V. Another notable difference is the change in the peak between 330 and 400 nm. In the 6$^{th}$ discharge data, this peak is symmetrical and centered at 350 nm, indicating a strong presence of the $S_6^{2-}$ species. However, during the charge, the peak transitions from symmetrical to asymmetrical shape, indicating the presence of $S_4^{2-}$ as the battery charges. This suggests that the $S_6^{2-}$ species are present in the electrolyte throughout both discharge and charge, while the $S_4^{2-}$ species are present during discharge until 1.90 V and reappear during charging between 2.30 and 2.60 V.

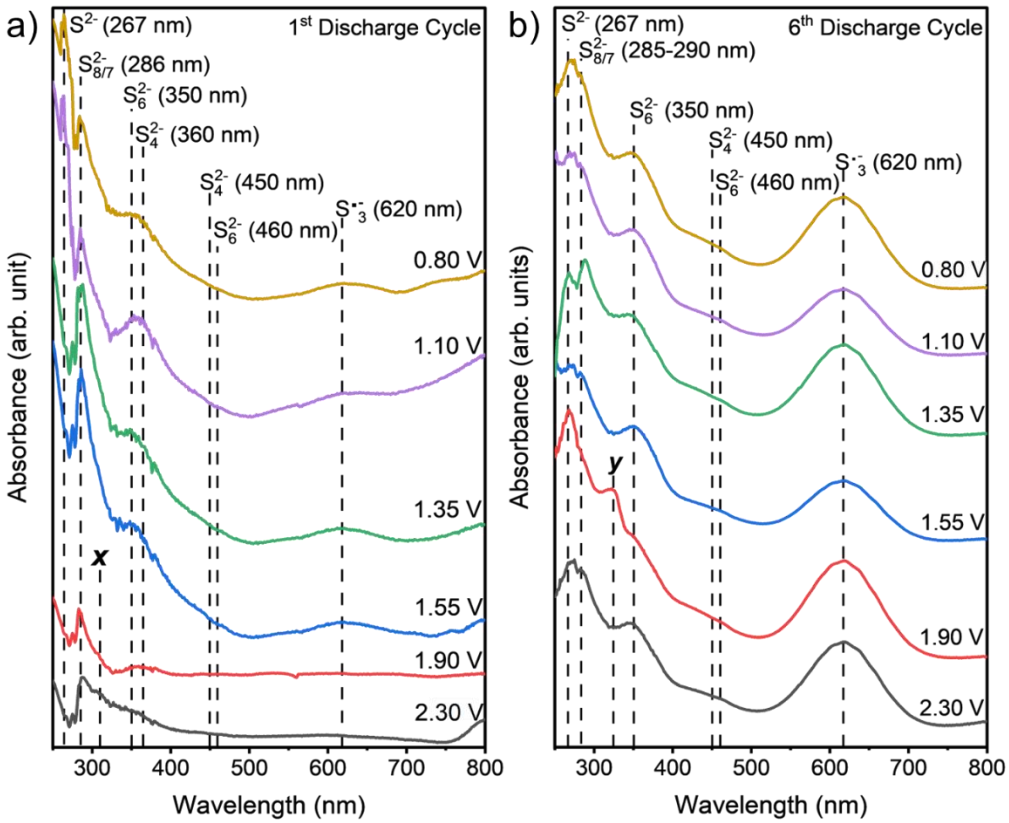


**Figure 4.** UV-Vis spectra of a) 1st discharge and b) 6th discharge of the Na-S battery at 0.1 C rate. The different PSs and their wavelengths are shown by vertically dashed lines.

### *In-situ* Raman spectroscopy results

To further investigate the reactions within the Na-S battery, *in-situ* Raman spectroscopy was conducted (see Experimental Methods). The results for measurements taken during the first discharge and charge cycle are shown in Figure 5 and Figure 6, respectively. The discharge data (Figure 5) shows that the 380 and 436 $cm^{-1}$ peaks appear at 2.60 V and remain until 1.80 V. The appearance of the 510 $cm^{-1}$ peak starts at 2.30 V and is present throughout the discharge data. These peaks indicate the presence of $Na_2S_8$ and $Na_2S_4$, respectively, from reference solutions in Figure 3. From 1.80 V, the peak at 380 $cm^{-1}$ shifts to 386 $cm^{-1}$ which could indicate the beginning of a comproportionation reaction between $Na_2S_8$ and $Na_2S_4$ to form $Na_2S_6$ (as $Na_2S_4$ is observed to be present before $Na_2S_6$ and this this corresponds to similar observations within Li-S). [52] This is seen in Figure 5a and more clearly in Figure 5b and c. In addition, in Figure 5c the peak at 440 $cm^{-1}$ changes shape becoming more symmetric with the 386 $cm^{-1}$ peak (these changes in peak shifts and shapes could indicate an increase in the presence of $Na_2S_6$). Meanwhile, the peak at 534 $cm^{-1}$ is related to the $S_3^{\bullet-}$ radical that first forms at 2.30 V and increases through the discharge cycle. It is also observed that the 192 $cm^{-1}$ peak first appears at 1.65 V, which could be related to the presence of $Na_2S_2$ (as indicated by the black dashed vertical line in Figure 5b). The presence of 192 $cm^{-1}$ peak corresponds to the second plateau in GCD curve and remains throughout the discharge step and in the final product. Finally, the 119 and 225 $cm^{-1}$ peaks begin to form at 1.10 V - indicating the formation of $Na_2S$. It is further noted that the intensity of the $Na_2S_4$ peak remains relatively constant after 2.22 V, while $Na_2S_6$ and $Na_2S_3$ peaks grow at lower potentials, even at 0.8 V. This behaviour aligns with the sequential polysulfide conversion reactions during discharge, where $Na_2S_6$ and $Na_2S_3$ formation intensifies as the system nears the end of discharge. The persistence of $Na_2S_4$ suggests it may be in equilibrium with other polysulfides, contributing to the overall conversion

mechanism.

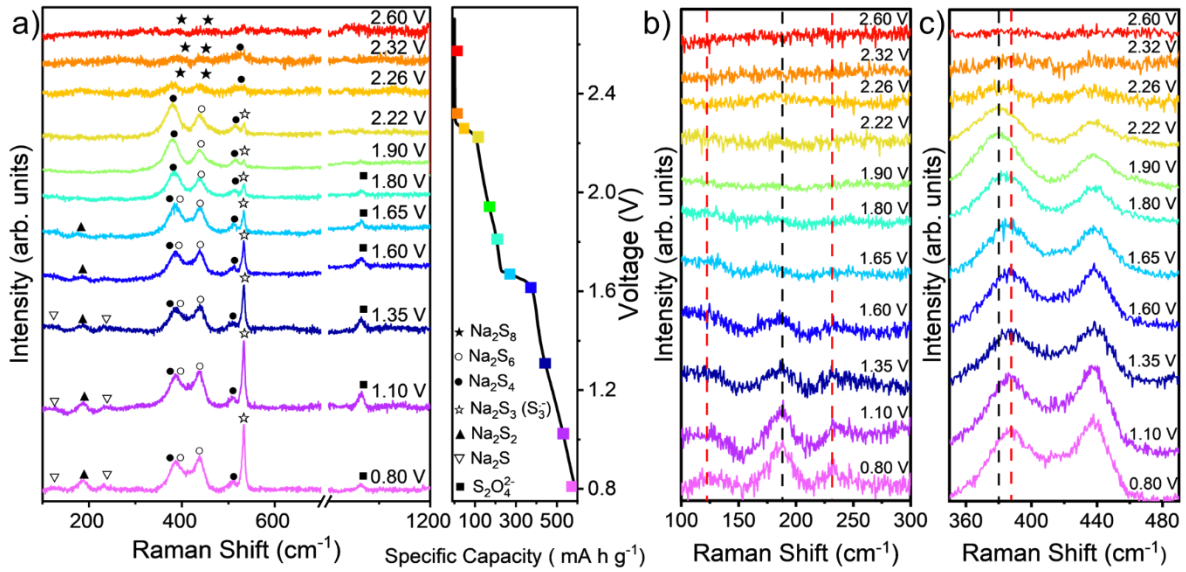


**Figure 5.** a) Experimental *in-situ* Raman spectra during galvanic discharge, presented with specific capacity per gram of sulfur. The spectra are color-coded to correspond to different voltage levels. The Raman cell was run at 0.1 C rate when data were being collected (see Methods). Characteristic peaks are labelled with assigned PS symbols at different voltages as indicated by the plot on the right side. Figure b) Zoomed in region between 100 and 300 $cm^{-1}$ of the Raman spectra showing the formation of $Na_2S_2$ and $Na_2S$. Specifically, presence of $Na_2S_2$ is indicated by the black dashed vertical line. The red vertical lines at 119 and 225 $cm^{-1}$ peaks indicate formation of $Na_2S$. c) Zoomed in region between 350 and 480 $cm^{-1}$ of the Raman spectra showing the peak shift signifying $Na_2S_8$ transforming to $Na_2S_6$ (peak shifting from red dashed line to the black one).

The charge data (Figure 6a) shows that between 0.80 V and 1.85 V, $Na_2S$ and $Na_2S_4$ convert back to higher-order PSs from the disappearance of peaks at 119 $cm^{-1}$, 225 $cm^{-1}$, and 510 $cm^{-1}$. It is also observed that $Na_2S_6$ can be reduced, but it should be noted that the peak at 386 $cm^{-1}$ does not shift back to 380 $cm^{-1}$ – suggesting that $Na_2S_6$ dissipates within the electrolyte and does not convert back to $Na_2S_8$. The data also show that the $S_3^{\bullet-}$ radical is present throughout,

indicating that it does not further reduce or convert and stays within the electrolyte. Additionally, $Na_2S_2$ is observed throughout, suggesting that $Na_2S_2$ is not easily reversible and could contribute to capacity decay.

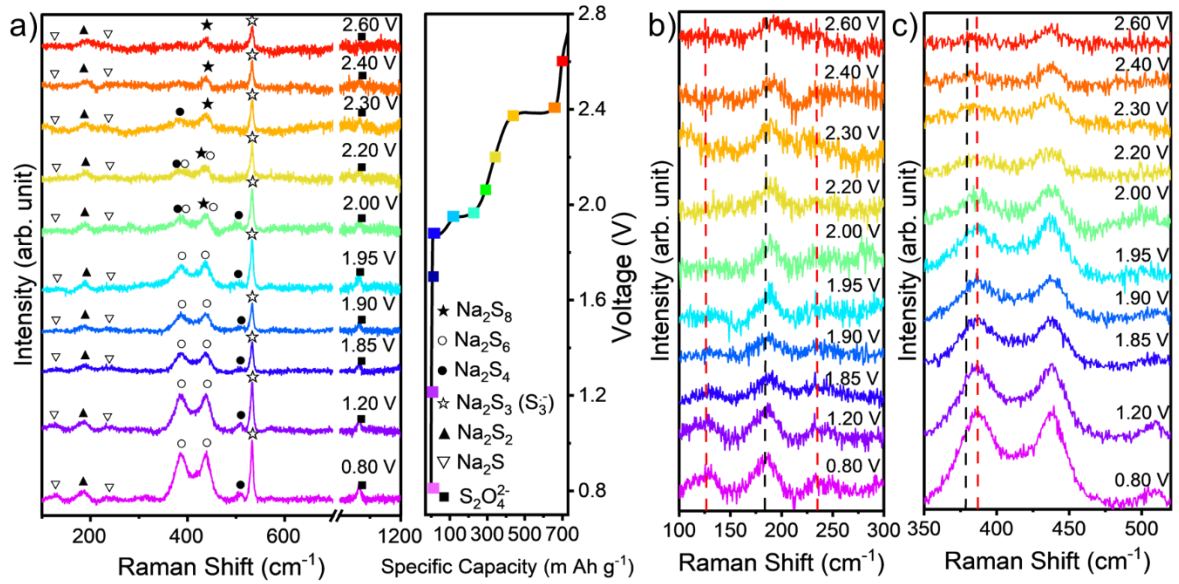


**Figure 6.** *In-situ* Raman measurements during charge cycle. a) Galvanic charge data, presented with specific capacity per gram of sulfur with the corresponding Raman spectra taken at each voltage. Characteristic peaks are labelled with assigned PS symbols at different voltages as indicated in the right figure. b) Zoomed in region between 100 and 300 $cm^{-1}$ of the Raman spectra. Specifically, the presence of $Na_2S_2$ is indicated by the black dashed vertical line. The red vertical lines at 119 and 225 $cm^{-1}$ peaks indicate formation of $Na_2S$. c) zoomed in region between 350 and 480 $cm^{-1}$.

Overall, Raman spectroscopy reveals that $Na_2S_6$ emerges at 2.22 V, a stage where both $Na_2S_8$ and $Na_2S_4$ exist. Notably, $Na_2S_6$ is absent in earlier discharge stages, suggesting it does not form directly from sulfur reduction but instead through disproportionation reactions: $Na_2S_8 \leftrightarrow Na_2S_6 + S_2$ and $2Na_2S_4 \leftrightarrow Na_2S_6 + Na_2S_2$. [40, 50, 51] The Raman signal for $S_3^{\bullet-}$ radicals intensifies during cycling, particularly when $Na_2S_4$ and $Na_2S_6$ are present, indicating the reactions $Na_2S_6 \leftrightarrow S_3^{\bullet-} + Na_2S_3$ and $2Na_2S_4 \leftrightarrow Na_2S_2 + 2\ S_3^{\bullet-}$. [40, 50, 51] This is further supported by UV-Vis

spectroscopy data which show absorption band shifts consistent with $S_3^{\bullet-}$ radical formation. The correlation between these spectral changes and the presence of $Na_2S_6$ and $Na_2S_4$ reinforces the role of disproportionation in the reaction mechanism.

**Discharge conversion mechanism**

We propose a discharge model shown in Figure 7 based on data collected from *ex-situ* UV-Vis and *in-situ* Raman spectroscopies. The model also includes the side reactions that cause loss in active material. Figure 7a shows a range of voltages at which the various NaPS species are found while Figure 7b shows the specific plateaus and the proposed reaction mechanisms. In particular, we observe a plateau at 2.30 V that is related to the formation of $Na_2S_8$ and $Na_2S_4$, and a second plateau at 1.60 V associated with the formation of $Na_2S_2$.

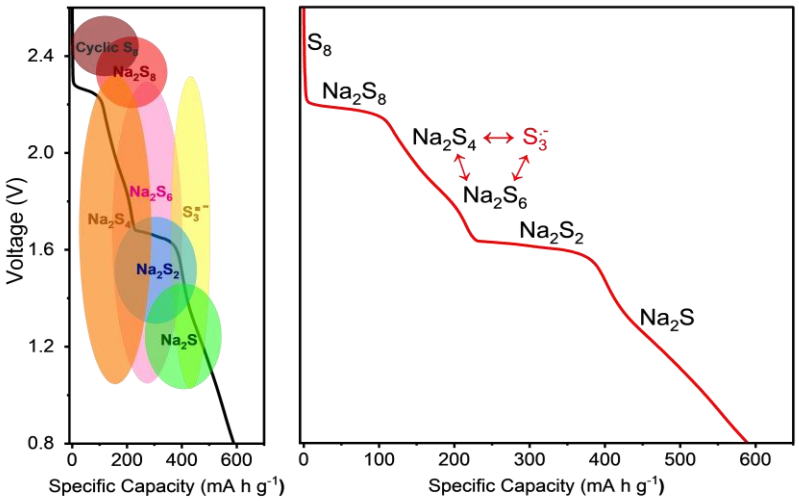


**Figure 7.** a) Galvanic charge curve of Na-S electrochemical cell showing the different species and their presence (indicated by shaded ellipses and circles) at different voltages. b) The same charge curve with corresponding pathways for sulfur reduction into different NaPS species with voltage. The stability and presence of various species were surmised from both *ex-situ* UV-Vis and *in-situ* Raman spectroscopies. Indicated in red is the loss of active material side reactions that occur during the sulfur reaction reaction.

## Conclusions

In conclusion, *ex-situ* UV-Vis and *in-situ* Raman spectroscopies were employed to determine the evolution of NaPS species during the charging and discharging of Na-S cells. $Na_2S_8$, $Na_2S_4$, $Na_2S_2$ were observed as key intermediates with $S_8$ as the starting product and $Na_2S$ as the final product. Our results suggest that intermediate $Na_2S_6$ does not contribute to the conversion mechanism. However, our results indicate that the formation of $Na_2S_6$ through a comproportionation reaction between $Na_2S_8$ and $Na_2S_4$ contributes to the loss of active material effect when charging. Further, our analysis points to $Na_2S_6$ contributing to the loss in active material by forming $S_3^{\bullet-}$ radicals through dissociation. The $S_3^{\bullet-}$ radical can also be formed by disproportionation of $Na_2S_4$. These processes exist in equilibrium within the electrolyte and typically result in the loss of active material to the electrolyte.

## Experimental Methods

### Preparation of the Reference Sodium Polysulfide Solutions and the Electrolyte

The electrolyte was prepared by dissolving sodium trifluoromethanesulfonate ($NaCF_3SO_3$) (Sigma-Aldrich) in tetraethylene glycol dimethyl ether (TEGDME) (Sigma Aldrich) solvent to form 1 M solution. 0.2 M NaPS solutions were prepared by reacting sodium sulfide ($Na_2S$) (Sigma Aldrich) with sulfur (Nanografi Nano Technology) in stoichiometric proportion in the electrolyte (5 mL). They were prepared and vigorously stirred for 24 h in an argon filled glovebox (<0.1 ppm $O_2$, <0.1 ppm $H_2O$).

### *Ex-Situ* UV-vis Measurements

UV-vis spectra for the reference solutions and the *ex-situ* study were obtained on a 2-channel spectrometer Lambda 750 (PerkinElmer) using argon-filled, sealed quartz glass cuvettes (Hellma Analytics, QS115). Each aliquot for UV-Vis analysis were taken non-destructively and subsequently returned to the system. The electrochemical study for *ex-situ* UV-Vis spectroscopy was conducted on a SP-50e potentiostat inside an argon filled glovebox. Electrochemical measurements were conducted at 0.1 C rate (1 C = 1672 mA h $g^{-1}$, normalised to the mass of sulfur) in a two-electrode configuration using metallic $MoS_2$/sulfur electrodes (12 mm diameter) and 16mm diameter sodium metal immersed in the electrolyte (30 mL). The aliquots were collected with a mechanical pipette (2 mL) at specified voltages.

### *In-Situ* Raman Measurements

The Raman spectra were obtained every 250 s using a Horiba LabRAM Odyssey and analysed through an ECC-Opto-Std-Aqu, El-Cell with a quartz viewing window. The reference polysulfides (PS) were recorded in the same set-up without the electrodes.

The electrochemical study for *in-situ* Raman spectroscopy was conducted using a Biologic SP-50e potentiostat. The set up used an airtight electrochemical cell (ECC-Opto-Std-Aqu, El-Cell) with a quartz glass viewing window. Electrochemical measurements were conducted at

0.1 C rate (1 C = 1672 mA h $g^{-1}$, normalised to the mass of sulfur) in a stacked two-electrode configuration. A top-to-bottom stack of metallic $MoS_2$/sulfur electrodes (10 mm diameter), glass fibre separator (10 mm diameter) and a sodium metal (12 mm diameter) were created and immersed with electrolyte (~1 mL).

**Synthesis of Metallic $MoS_2$ Nanosheets and Electrodes**

Lithiation of 2H-$MoS_2$ (0.6 g, < 2 μm particle size, Alfa Aesar) was carried out with the n-butyllithium in hexane solution (6 mL, 1.6 M, Sigma Aldrich) and hexane (60 mL, 99% purity). [53] The solution was stirred at 60 RPM at 80 °C for 72 h under reflux. After cooling the product, it was washed with hexane twice (95% purity, 2 x 50 mL). The product was then dried in a vacuum oven (60 °C,12 h) and stored in an argon-filled glovebox (<0.1 ppm $O_2$, <0.1 ppm $H_2O$).

**Fabrication of the Cathode.**

The bulk synthesised product of $Li_xMoS_2$ was exfoliated into nanosheets in tetrahydrofuran (THF) (0.5 mg/mL) via sonication for 1 h in an ice bath. Then the product was filtered and dried. The cathode was prepared by sonicating 40:60:10 mass ratio of 1T-$Li_xMoS_2$ or carbon, sulfur and polyvinylidene fluoride (PVDF) in a NMP for 10 min. The resultant solution was stirred for 24 h until the solution was homogeneous. Then, the solution was doctor bladed (150 μm thickness) onto carbon-coated aluminium foil, dried for 24 h at 60 °C under vacuum, and cut into electrodes (12 mm diameter). The volumetric sulfur loading was calculated via the weight of electrodes.

**Electrochemical Characterization**

**Assembly and Testing of Coin Cells**

The electrochemical performance of the $Li_xMoS_2$-based cathodes was evaluated in coin cells (CR2032, Cambridge Energy Solutions), which were assembled in an argon-filled glovebox. The assembly included the components: 12 mm diameter $Li_xMoS_2$/sulfur cathode, 16 mm

diameter sodium chip, a glass fibre separator, and the electrolyte as prepared previously (flooding the separator with electrolyte). The electrochemical measurements for the coin cells were conducted on a battery cycler (LANDT CT3002A, 1U). GCD tests were performed in the voltage range of 2.6 V to 0.8 V at 0.1 C rate (1 C = 1672 mA h $g^{-1}$, normalised to the mass of sulfur).

**Author Information**

**Corresponding Author**

**Manish Chhowalla**

Department of Materials Science and Metallurgy, University of Cambridge, Cambridge, UK

Email: mc209@cam.ac.uk

**Authors**

**Esther Lilian Gray**

Department of Materials Science and Metallurgy, University of Cambridge, Cambridge, UK

**Jung-In Lee**

Department of Materials Science and Metallurgy, University of Cambridge, Cambridge, UK

**Zhuangnan Li**

Department of Materials Science and Metallurgy, University of Cambridge, Cambridge, UK

**James Moloney**

Department of Materials Science and Metallurgy, University of Cambridge, Cambridge, UK

**Ziwei Jeffrey Yang**

Department of Materials Science and Metallurgy, University of Cambridge, Cambridge, UK

**Author Contributions**

M.C. conceived and designed the research; E.L.G, J.L., and Z.L. performed the experiments and the characterization of the materials; E.L.G and M.C. analyzed the data and E.L.G., J.M., M.C., and Z.L. wrote the manuscript with input from all co-authors. All authors have given approval to the final version of the manuscript.

**Acknowledgement**

This research was supported by the Faraday Institution's LiSTAR program. E.L.G would like the Faraday Institution for her Doctoral Fellowship. E.L.G would like to thank Liam Hallinan who provided mentorship as a learning support guide. We thank Prof Rachel Evans' Photoactive Materials Group in the Department for access to the UV-Vis spectrometer. We acknowledge the support from the Henry Royce Institute. Z.L. acknowledges the financial support and Research Fellowship from the Herchel Smith Fund and King's College, Cambridge.

**Supporting Information Available:** Additional materials characterization, battery analysis, complementary reference database for UV-Vis and Raman data are available.

**References**

(1) König, A.; Nicoletti, L.; Schröder, D.; Wolff, S.; Waclaw, A.; Lienkamp, M. An Overview of Parameter and Cost for Battery Electric Vehicles. *In World Electric Vehicle Journal*, **2021**; Vol. 12.

(2) Manthiram, A.; Fu, Y.; Su, Y.-S. Challenges and Prospects of Lithium–Sulfur Batteries. *Accounts of Chemical Research* **2013**, *46* (5), 1125-1134.

(3) Kumar, D.; Kuhar, S. B.; Kanchan, D. K. Room temperature sodium-sulfur batteries as emerging energy source. *Journal of Energy Storage* **2018**, *18*, 133-148.

(4) Dong, C.; Zhou, H.; Liu, H.; Jin, B.; Wen, Z.; Lang, X.; Li, J.; Kim, J.; Jiang, Q. Inhibited shuttle effect by functional separator for room-temperature sodium-sulfur batteries. *Journal of Materials Science & Technology* **2022**, *113*, 207-216.

(5) Yu, X.; Manthiram, A. Performance Enhancement and Mechanistic Studies of Room-Temperature Sodium–Sulfur Batteries with a Carbon-Coated Functional Nafion Separator and a Na2S/Activated Carbon Nanofiber Cathode. *Chemistry of Materials* **2016**, *28* (3), 896-905.

(6) Xu, J.; Qiu, Y.; Yang, J.; Li, H.; Han, P.; Jin, Y.; Liu, H.; Sun, B.; Wang, G. Review of Separator Modification Strategies: Targeting Undesired Anion Transport in Room Temperature Sodium–Sulfur/Selenium/Iodine Batteries. *Advanced Functional Materials* **2024**, *34* (2), 2306206.

(7) Xu, X.; Zhou, D.; Qin, X.; Lin, K.; Kang, F.; Li, B.; Shanmukaraj, D.; Rojo, T.; Armand, M.; Wang, G. A room-temperature sodium–sulfur battery with high capacity and stable cycling performance. *Nature Communications* **2018**, *9* (1), 3870.

(8) Ryu, H.; Kim, T.; Kim, K.; Ahn, J.-H.; Nam, T.; Wang, G.; Ahn, H.-J. Discharge reaction mechanism of room-temperature sodium–sulfur battery with tetra ethylene glycol dimethyl ether liquid electrolyte. *Journal of Power Sources* **2011**, *196* (11), 5186-5190.

(9) Seh, Z. W.; Sun, J.; Sun, Y.; Cui, Y. A Highly Reversible Room-Temperature Sodium Metal Anode. *ACS Central Science* **2015**, *1* (8), 449-455.

(10) Chen, J.; Zhang, H.; Fang, M.; Ke, C.; Liu, S.; Wang, J. Design of Localized High-Concentration Electrolytes via Donor Number. *ACS Energy Letters* **2023**, *8* (4), 1723-1734.

(11) Yan, Z.; Zhao, L.; Wang, Y.; Zhu, Z.; Chou, S.-L. The Future for Room-Temperature Sodium–Sulfur Batteries: From Persisting Issues to Promising Solutions and Practical Applications. *Advanced Functional Materials* **2022**, *32* (36), 2205622.

(12) Ghosh, A.; Shukla, S.; Monisha, M.; Kumar, A.; Lochab, B.; Mitra, S. Sulfur Copolymer: A New Cathode Structure for Room-Temperature Sodium–Sulfur Batteries. *ACS Energy Letters* **2017**, *2* (10), 2478-2485.

(13) Hwang, T. H.; Jung, D. S.; Kim, J.-S.; Kim, B. G.; Choi, J. W. One-Dimensional Carbon–Sulfur Composite Fibers for Na–S Rechargeable Batteries Operating at Room Temperature. *Nano Letters* **2013**, *13* (9), 4532-4538.

(14) Xin, S.; Yin, Y.-X.; Guo, Y.-G.; Wan, L.-J. A High-Energy Room-Temperature Sodium-Sulfur Battery. *Advanced Materials* **2014**, *26* (8), 1261-1265.

(15) Kumar, A.; Ghosh, A.; Forsyth, M.; MacFarlane, D. R.; Mitra, S. Free-Radical Catalysis and Enhancement of the Redox Kinetics for Room-Temperature Sodium–Sulfur Batteries. *ACS Energy Letters* **2020**, *5* (6), 2112-2121.

(16) Wang, Y.; Zhou, D.; Palomares, V.; Shanmukaraj, D.; Sun, B.; Tang, X.; Wang, C.; Armand, M.; Rojo, T.; Wang, G. Revitalising sodium–sulfur batteries for non-high-temperature operation: a crucial review. *Energy & Environmental Science* **2020**, *13* (11), 3848-3879.

(17) Yu, X.; Manthiram, A. Room-Temperature Sodium–Sulfur Batteries with Liquid-Phase Sodium Polysulfide Catholytes and Binder-Free Multiwall Carbon Nanotube Fabric Electrodes. *The Journal of Physical Chemistry C* **2014**, *118* (40), 22952-22959.

(18) Kim, I.; Park, J.-Y.; Kim, C.; Park, J.-W.; Ahn, J.-P.; Ahn, J.-H.; Kim, K.-W.; Ahn, H.-J. Sodium polysulfides during charge/discharge of the room-temperature Na/S battery using TEGDME electrolyte. *Journal of The Electrochemical Society* **2016**, *163* (5), A611.

(19) Yan, Z.; Liang, Y.; Xiao, J.; Lai, W.; Wang, W.; Xia, Q.; Wang, Y.; Gu, Q.; Lu, H.; Chou, S.-L.; et al. A High-Kinetics Sulfur Cathode with a Highly Efficient Mechanism for Superior Room-Temperature Na–S Batteries. *Advanced Materials* **2020**, *32* (8), 1906700.

(20) Guo, Q.; Li, S.; Liu, X.; Lu, H.; Chang, X.; Zhang, H.; Zhu, X.; Xia, Q.; Yan, C.; Xia, H. Ultrastable Sodium–Sulfur Batteries without Polysulfides Formation Using Slit Ultramicropore Carbon Carrier. *Advanced Science* **2020**, *7* (11), 1903246.

(21) Wang, Y.; Zhang, Y.; Cheng, H.; Ni, Z.; Wang, Y.; Xia, G.; Li, X.; Zeng, X. Research Progress toward Room Temperature Sodium Sulfur Batteries: A Review. *In Molecules*, 2021; Vol. 26.

(22) Yu, X.; Manthiram, A. Capacity Enhancement and Discharge Mechanisms of Room-Temperature Sodium–Sulfur Batteries. *ChemElectroChem* **2014**, *1* (8), 1275-1280.

(23) Carter, R.; NewRingeisen, A.; Reed, D.; Atkinson, R. W., III; Mukherjee, P. P.; Love, C. T. Optical Microscopy Reveals the Ambient Sodium–Sulfur Discharge Mechanism. *ACS Sustainable Chemistry & Engineering* **2021**, *9* (1), 92-100.

(24) Li, Z.; Sami, I.; Yang, J.; Li, J.; Kumar, R. V.; Chhowalla, M. Lithiated metallic molybdenum disulfide nanosheets for high-performance lithium–sulfur batteries. *Nature Energy* **2023**.

(25) Liu, Y.; Bettels, F.; Lin, Z.; Li, Z.; Shao, Y.; Ding, F.; Liu, S.; Zhang, L. Recent Advances in Transition-Metal-Based Catalytic Material for Room-Temperature Sodium–Sulfur Batteries. *Advanced Functional Materials* **2024**, *34* (5), 2302626.

(26) Taiwo, G. S.; Rashti, A.; Mishra, M.; Yao, K. P. C. Polysulfide Speciation in Li–S Battery Electrolyte via In-Operando Optical Imaging and Ex-Situ UV-vis Spectra Analysis. *Journal of The Electrochemical Society* **2022**, *169* (9), 090518.

(27) Han, D.-H.; Kim, B.-S.; Choi, S.-J.; Jung, Y.; Kwak, J.; Park, S.-M. Time-Resolved In Situ Spectroelectrochemical Study on Reduction of Sulfur in N , N′-Dimethylformamide. *Journal of The Electrochemical Society* **2004**, *151* (9), E283.

(28) Tobishima, S.-I.; Yamamoto, H.; Matsuda, M. Study on the reduction species of sulfur by alkali metals in nonaqueous solvents. *Electrochimica Acta* **1997**, *42* (6), 1019-1029.

(29) Manan, N. S. A.; Aldous, L.; Alias, Y.; Murray, P.; Yellowlees, L. J.; Lagunas, M. C.; Hardacre, C. Electrochemistry of Sulfur and Polysulfides in Ionic Liquids. *The Journal of Physical Chemistry B* **2011**, *115* (47), 13873-13879.

(30) Ledé, B.; Demortier, A.; Gobeltz-Hautecœur, N.; Lelieur, J. P.; Picquenard, E.; Duhayon, C. Observation of the ν3 Raman band of S3− inserted into sodalite cages. *Journal of Raman Spectroscopy* **2007**, *38* (11), 1461-1468.

(31) Yu, X.; Manthiram, A. Highly Reversible Room-Temperature Sulfur/Long-Chain Sodium Polysulfide Batteries. *The Journal of Physical Chemistry Letters* **2014**, *5* (11), 1943-1947.

(32) Bonnaterre, R.; Cauquis, G. Spectrophotometric study of the electrochemical reduction of sulphur in organic media. *Journal of the Chemical Society, Chemical Communications* **1972**, (5), 293-294.

(33) Martin, R. P.; Doub, W. H., Jr.; Roberts, J. L., Jr.; Sawyer, D. T. Electrochemical reduction of sulfur in aprotic solvents. *Inorganic Chemistry* **1973**, *12* (8), 1921-1925.

(34) Kim, B. S.; Park, S. M. In Situ Spectroelectrochemical Studies on the Reduction of Sulfur in Dimethyl Sulfoxide Solutions. *Journal of The Electrochemical Society* **1993**, *140* (1), 115.

(35) Wen, Q.; Wu, Y.; Wang, X.; Zhuang, Z.; Yu, Y. Researches on preparation and properties of sodium polysulphide as gold leaching agent. *Hydrometallurgy* **2017**, *171*, 77-85.

(36) Wang, Y.; Luo, Z.; Liu, D.; Li, Y. Immobilization of mercury in tailings originating from the historical artisanal and small-scale gold mining using sodium polysulfide. *Environmental Science and Pollution Research* **2022**, *29*, 1-17.

(37) Kandhasamy, S.; Nikiforidis, G.; Jongerden, G.; Jongerden, F.; Sanden, M. C. M.; Tsampas, M. Operational strategies to improve the performance and long-term cyclability of intermediate temperature sodium-sulfur (IT-NaS) battery. *ChemElectroChem* **2021**, *8*.

(38) Janz, G. J.; Downey, J. R.; Roduner, E.; Wasilczyk, G. J.; Coutts, J. W.; Eluard, A. Raman studies of sulfur-containing anions in inorganic polysulfides. Sodium polysulfides. *Inorganic Chemistry* **1976**, *15* (8), 1759-1763.

(39) El Jaroudi, O.; Picquenard, E.; Gobeltz, N.; Demortier, A.; Corset, J. Raman Spectroscopy Study of the Reaction between Sodium Sulfide or Disulfide and Sulfur: Identity of the Species Formed in Solid and Liquid Phases. *Inorganic Chemistry* **1999**, *38* (12), 2917-2923.

(40) Chivers, T.; Lau, C. Raman spectroscopic identification of the S4N-and S3-ions in blue solutions of sulfur in liquid ammonia. *Inorganic Chemistry* **1982**, *21* (1), 453-455.

(41) McBrayer, J. D.; Beechem, T. E.; Perdue, B. R.; Apblett, C. A.; Garzon, F. H. Polysulfide Speciation in the Bulk Electrolyte of a Lithium Sulfur Battery. *Journal of The Electrochemical Society* **2018**, *165* (5), A876.

(42) Hagen, M.; Schiffels, P.; Hammer, M.; Dörfler, S.; Tübke, J.; Hoffmann, M. J.; Althues, H.; Kaskel, S. In-Situ Raman Investigation of Polysulfide Formation in Li-S Cells. *Journal of The Electrochemical Society* **2013**, *160* (8), A1205.

(43) Daly, F. P.; Brown, C. W. Raman spectra of sodium tetrasulfide in primary amines. Evidence for sulfide (S42-and S8n-) ions in rhombic sulfur-amine solutions. *The Journal of Physical Chemistry* **1975**, *79* (4), 350-354.

(44) Wu, H.-L.; Huff, L. A.; Gewirth, A. A. In Situ Raman Spectroscopy of Sulfur Speciation in Lithium–Sulfur Batteries. *ACS Applied Materials & Interfaces* **2015**, *7* (3), 1709-1719.

(45) Janz, G. J.; Coutts, J. W.; Downey, J. R.; Roduner, E. Raman studies of sulfur-containing anions in inorganic polysulfides. Potassium polysulfides. *Inorganic Chemistry* **1976**, *15* (8), 1755-1759.

(46) Dubois, P.; Lelieur, J. P.; Lepoutre, G. Identification and characterization of lithium polysulfides in solution in liquid ammonia. *Inorganic Chemistry* **1988**, *27* (1), 73-80.

(47) Chivers, T. Ubiquitous trisulphur radical ion S3−·. *Nature* **1974**, *252* (5478), 32-33.

(48) Chivers, T.; Elder, P. J. W. Ubiquitous trisulfur radical anion: fundamentals and applications in materials science, electrochemistry, analytical chemistry and geochemistry. *Chemical Society Reviews* **2013**, *42* (14), 5996-6005.

(49) Holzer, W.; Murphy, W. F.; Bernstein, H. J. Resonance raman effect of S3− doped in a NaCl single crystal. *Chemical Physics Letters* **1970**, *4* (10), 641-642.

(50) Chivers, T.; Elder, P. J.; Ubiquitous trisulfur radical anion: fundamentals and applications in materials science, electrochemistry, analytical chemistry and geochemistry. *Chemical Society Reviews* **2013**, 42 (14), 5996-6005.

(51) Chivers, T.; Ubiquitous trisulphur radical ion S3−·. *Nature* **1974**, 252 (5478), 32-33.

(52) Liu, R.; Wei, Z.; Peng, L.; Zhang, L.; Zohar, A.; Schoeppner, R.; Wang, P.; Wan, C.; Zhu, D.; Liu, H.; et al. Establishing reaction networks in the 16-electron sulfur reduction reaction. *Nature* **2024**, *626* (7997), 98-104. DOI: 10.1038/s41586-023-06918-4.

(53) Voiry, D.; Mohite, A.; Chhowalla, M. Phase engineering of transition metal dichalcogenides. *Chemical Society Reviews* **2015**, *44* (9), 2702-2712.

## Table of Contents Only